

## Wireless actuation of bulk acoustic modes in micromechanical resonators

Farrukh Mateen,<sup>1</sup> Benjamin Brown,<sup>2</sup> Shyamsunder Erramilli,<sup>3,4</sup> and Pritiraj Mohanty<sup>3,a)</sup>

<sup>1</sup>*Department of Mechanical and Aerospace Engineering, Boston University, 110 Cummington Street, Boston, Massachusetts 02215, USA*

<sup>2</sup>*Department of Electrical and Computer Engineering, Boston University, 8 St. Mary's St., Boston, Massachusetts 02215, USA*

<sup>3</sup>*Department of Physics, Boston University, 590 Commonwealth Avenue, Boston, Massachusetts 02215, USA*

<sup>4</sup>*Department of Biomedical Engineering and Photonics Center, Boston University, 8 St. Mary's St, Boston, Massachusetts 02215, USA*

(Received 5 July 2016; accepted 4 August 2016; published online 16 August 2016)

We report wireless actuation of a Lamb wave micromechanical resonator from a distance of over 1 m with an efficiency of over 15%. Wireless actuation of conventional micromechanical resonators can have broad impact in a number of applications from wireless communication and implantable biomedical devices to distributed sensor networks. *Published by AIP Publishing.*

[<http://dx.doi.org/10.1063/1.4961247>]

Wireless actuation of micro- and nano-mechanical resonators is of tremendous fundamental and technical interests, as these resonators are often the building blocks of countless devices such as filters, oscillators, accelerometers, and gyroscopes in wireless communication, mass balance, biosensors, and wireless power receiving elements in implantable biomedical devices. Efficient wireless actuation of the building-block resonators can therefore enable wireless operation of these devices. For instance, a biomedical device implanted in the body can be actuated or powered, and controlled and manipulated from outside, non-invasively, without the use of hard wiring. Furthermore, sub-millimeter footprint of these resonators could be important for applications such as brain implants, where small size is necessary for accurate and highly localized targets. Similarly, in a very different application of distributed sensor networks, both size and power are critical factors in determining viability of the underlying technology.

Micromechanical acoustic piezoelectric resonators<sup>1-5</sup> employ inverse piezoelectric effect for actuation. An applied electric field causes a mechanical strain/stress in the material upon application of an electric field across it, exciting an acoustic wave. Conversely, direct piezoelectric effect converts mechanical vibrations resulting from an acoustic wave into a proportional electric charge polarization, which can be used to sense the acoustic wave.

Conventionally, acoustic wave resonators have been confined to the realms of either Bulk Acoustic Waves (BAW) or Surface Acoustic Waves (SAW) resonators depending on whether the wave travels through the bulk or on the surface of the piezoelectric resonator, respectively. Recently, thin plate modes called Lamb waves resonators (LWRs) have been developed. These resonators combine the best of both the SAW and BAW technologies to enable devices that are easy to fabricate and foundry compatible. The LWRs typically have high quality factors (Q), robust thermal compensation, low noise floor and high frequency of operation.<sup>6-11</sup> These thin plate guided waves are a type of ultrasonic waves that

remain guided between the upper and lower surfaces of a piezoelectric plate, and thus are able to travel longer distances with little attenuation. These waves propagate in piezoelectric plates that are thinner in comparison to the wavelength of the wave being transduced by the Inter-Digitated Transducers (IDTs) patterned on top of the piezoelectric resonator. Suspension of the structure enables a higher Q and larger phase velocity (which enables higher frequency of operation).

Lamb waves are further classified into symmetric ( $S_0$ ,  $S_1$ ,  $S_2$ , etc.) or antisymmetric ( $A_0$ ,  $A_1$ ,  $A_2$ , etc.) modes, indicating the symmetry of a particle's displacement relative to an imaginary median plane drawn through the thickness of the plate. The symmetric modes are also called longitudinal or contour modes because the average displacement over the thickness of the plate or layer is in the longitudinal direction. While the anti-symmetric modes are observed to exhibit average displacements in the transverse direction, these are called flexural modes. Due to their high phase velocity, weak dispersion, low susceptibility to mode conversion, and moderate electromechanical coupling, the lowest-order symmetric mode ( $S_0$ ) has found most use in many practical fields such as high temperature sensing applications,<sup>12</sup> high frequency wireless communications,<sup>13</sup> chemical and biological sensing,<sup>14,15</sup> pressure and gravimetric sensing,<sup>16,17</sup> and structural health monitoring.<sup>18</sup> Given the importance of the  $S_0$  mode for practical applications, here we demonstrate the excitation of the  $S_0$  mode wirelessly using the recent demonstration of a novel wireless actuation technique employing piezoelectric resonators.<sup>19</sup>

Figure 1(a) is an optical micrograph showing the top-view of the MEMS piezoelectric resonator employed for this study. The central rectangular plate (shown in blue color) is the piezoelectric element of size  $266 \mu\text{m} \times 166 \mu\text{m}$ , which is suspended over a slightly larger rectangular cavity. The resonator is connected to the bulk material via thin rectangular connects. The top of the resonating element is overlaid with five,  $15\text{-}\mu\text{m}$  wide, gold interdigitated transducers (IDTs), shown in dull gold color. Three of these IDTs are connected via a thin gold track to the RF-1 tab on one side (not shown) while the other two IDTs are connected to the RF-2 tab on

<sup>a)</sup>Email: mohanty@physics.bu.edu

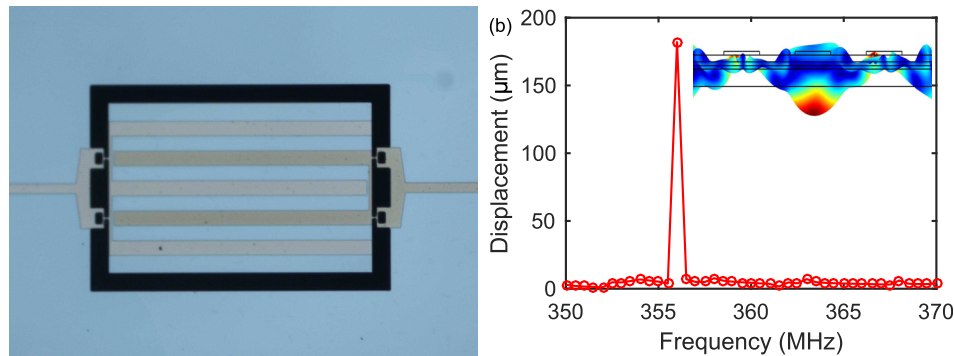


FIG. 1. (a) Top view of the micromechanical piezoelectric resonator. The plate-type piezoelectric element of the resonator has a lateral dimension of  $266 \mu\text{m} \times 166 \mu\text{m}$ . Five interdigitated transducers (IDTs) are overlaid on this element with three connected to the RF-1 tab (not shown) though thin connects on one side while the remaining two are connected similarly to the RF-2 tab (not shown) on the opposite side. The device can be piezoelectrically excited via the application of an ac-signal to either of the RF-1 or 2 tabs. (b) The displacement vs. frequency sweep plot produced by COMSOL simulation depicts a mode at the 356 MHz frequency. The inset depicts the symmetric lamb wave mode shape as simulated by COMSOL multiphysics.

the other side (not shown) via a similar thin gold track. An ac-signal can either be applied to the RF-1 or RF-2 tabs to piezoelectrically actuate the resonator while the other tab can be used to measure the output of the device. These resonators are fabricated by standard microfabrication methods. The total thickness of the resonator is  $10\text{-}\mu\text{m}$ . From bottom to top, it consists of a  $5\text{-}\mu\text{m}$  base polysilicon layer, a  $1\text{-}\mu\text{m}$  layer of silicon oxide, a  $1\text{-}\mu\text{m}$  layer of molybdenum ground-electrode, a  $2\text{-}\mu\text{m}$  layer of aluminum nitride (AlN), and a  $1\text{-}\mu\text{m}$  layer of patterned molybdenum top-electrodes.

The top IDTs of a piezoelectric resonator (shown in dull-gold color in Figure 1(a)) can act as inherent patch antennas which can couple with and receive energy from on-coming time varying electric fields produced by a source antenna at a distance. In this paper, we demonstrate wireless actuation of the symmetric Lamb-wave mode  $S_0$  using the piezoelectric resonator in Figure 1(a).

First, a 2-D model conforming to the approximate dimensions of the device, shown in Figure 1(a), was developed and simulated using the piezoelectric module in the frequency domain of the COMSOL Multiphysics package. The simulation swept the frequency between 350 MHz and 370 MHz and calculated the deformation of the device at every mesh point. The results revealed a mode at 356 MHz, as shown in Figure 1(b). At this frequency, the deformation of the device resembled the mode shape expected from the symmetric Lamb wave mode  $S_0$ . The inset in Figure 1(b) depicts this mode shape.

The frequency  $f_l$  of the  $S_0$  mode is theoretically calculated to be about 368 MHz and is dependent on the longitudinal velocity of sound  $v_l$  through the resonator structure of thickness  $d$  comprised of the layers as described before and given as follows:

$$f_l = \frac{v_l}{2d}. \quad (1)$$

The sound velocity  $v_l$  through the stack of thickness  $d$  is calculated to be about 7368 m/s using the following equation:

$$v_l = \sqrt{\frac{E_l}{\rho}}. \quad (2)$$

Here,  $E_l$  is the longitudinal Young's modulus and  $\rho$  is the density of the stack. A Voigt model for weighted averages is assumed as a first-order approximation for the Young's modulus of the stack given as follows:

$$E_l = E_1V_{f1} + E_2V_{f2} + E_3V_{f3} + E_4V_{f4} + E_5V_{f5}, \quad (3)$$

where  $E_1$  to  $E_5$  and  $V_{f1}$  to  $V_{f5}$  are the Young's moduli and volume fractions of polysilicon base layer, silicon dioxide, molybdenum ground layer, aluminum nitride, and molybdenum top electrodes, respectively. The volume fractions of each layer is the ratio of the volume of that specific layer to that of the total volume of the entire stack. Thus, for the device shown in Figure 1(a),  $E_l$  is calculated to be 201.82 GPa. In addition, replacing all the  $E$ 's with  $\rho_1$  to  $\rho_5$  (which are the respective densities of the stack in similar order as before) in Equation (3) yields an estimate for the stack density ( $\rho$ ), which comes out to be approximately  $3718 \text{ kg/m}^3$ . It may be noted that the Voigt weighted average method imposes the highest limit on the Young's modulus for a stack of given dimensions and thickness. Hence, the resulting frequency calculated from it is an overestimate of the actual frequency.

The resonator was excited using a Vector Network Analyzer (VNA, Agilent N3383) and a resonance peak at 356.2 MHz was observed. Figure 2(a) shows the S21 parameter (in dB) in the range of 353 MHz and 360 MHz. Figure 2(b) shows the resonance plot of the S21 (in dB) data in the same frequency range with the device mounted on a stage facing directly towards a source antenna, at a distance of 0.50 m. The device is indeed actuated wirelessly at exactly the same frequency of 356.2 MHz, thus confirming wireless actuation method. Henceforth, similar measurements were carried out for all distances between the source antenna and the piezoelectric device from 0.15 m up to 1.25 m. It may be noted that all wireless actuation measurements are carried out at a fixed source antenna power of  $-10 \text{ dBm}$  (0.1 mW). A Labview program swept the VNA frequency between 353 MHz and 360 MHz and recorded the resulting S21 data for each distance. The S21 parameter represents the ratio of the voltage amplitude at port 2 (response from the resonator device) of the VNA with respect to that at port 1 (excitation to source antenna).

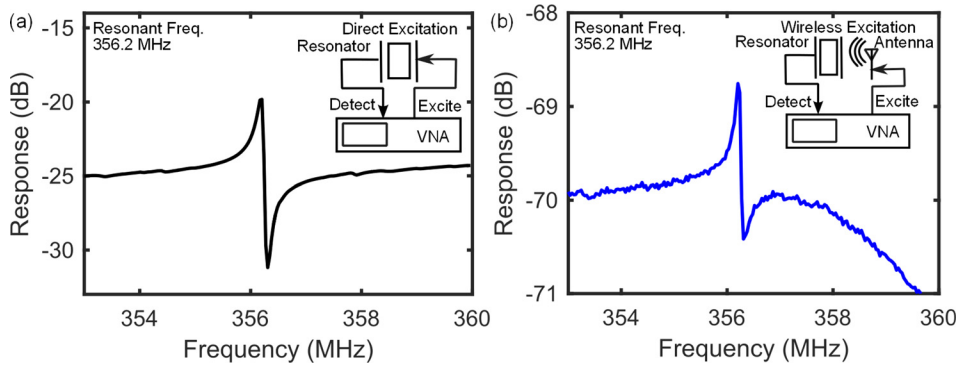


FIG. 2. (a) Response of the device actuated and measured by direct actuation via the VNA, as depicted by the inset schematic, shows a resonance peak at 356.2 MHz. (b) The response of the device under wireless actuation as depicted by the inset schematic. A similar peak is detected at 356.2 MHz, confirming wireless actuation of the device.

Piezoelectric resonators are conventionally modeled in terms of equivalent lumped elements of a Butterworth Van Dyke (BVD) model. The real part of the admittance ( $G_{BVD}$ ) is the Lorentzian response of the resonator, which is extracted by a MATLAB program as given in the following equation:

$$G_{BVD} = \frac{R_m}{R_m^2 + \left(\omega L_m - \frac{1}{\omega C_m}\right)^2} \quad (4)$$

Here,  $R_m$ ,  $L_m$ , and  $C_m$  are the equivalent BVD circuit resistance ( $\Omega$ ), inductance (H), and capacitance (F), which represent the mechanical motion of the piezoelectric resonator, and  $\omega$  is the angular frequency (rad/s). From the equation, it can be seen that at resonance when  $\omega$  is equal to the natural frequency,  $G_{BVD}$  will be maximum and only be limited by the value “ $1/R_m$ ” while the inductance  $L_m$  and capacitance

$C_m$  cancel each other. The value of  $G_{BVD}$  at resonance is extracted and plotted against its respective distance given in terms of the wavelength ( $\lambda$ ) (about 0.8 m calculated at the resonance frequency of 356.2 MHz), between the measured 0.15 m and 1.25 m distance range in Figure 3(a). While it is expected that the curve will show a steady decline as the distance of the device increases from the source antenna instead anomalous peaks and troughs are observed, consistent with near-field effects. Although the device actuates wirelessly, this counterintuitive distance dependence is due to the near-field (operation within one wavelength) regime effects where linearly polarized systems are susceptible to reflections and multipath interferences. In a separate COMSOL simulation (see supplementary material in Ref. 19), similar anomalous peaks have been observed in the distance dependence response, which provide credence to the claim that near field regime does cause the counterintuitive response observed. The distance (given in terms of the wavelength) dependence

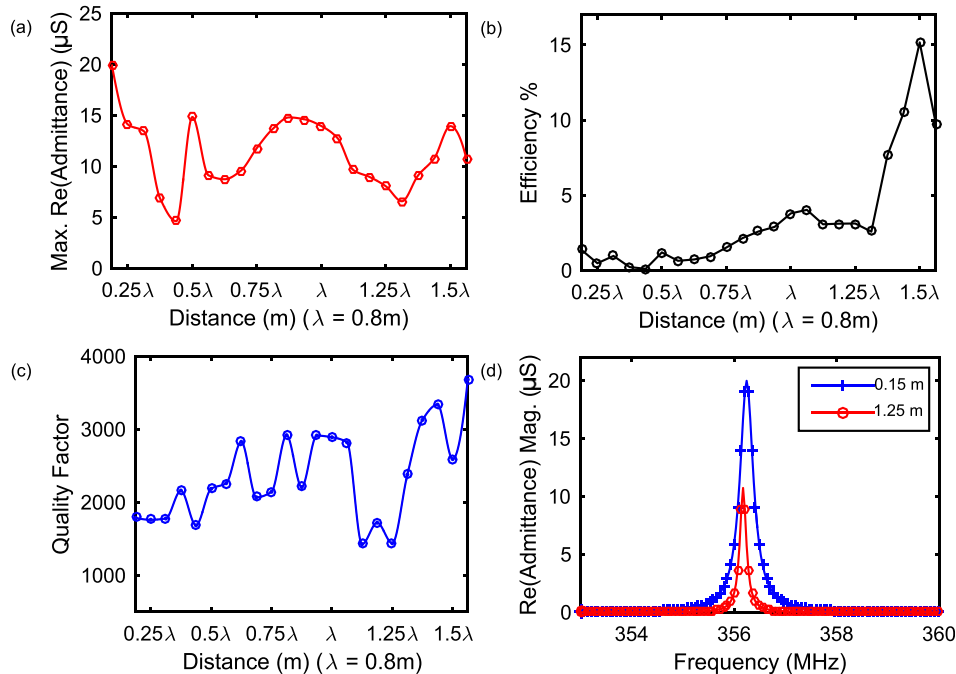


FIG. 3. (a) The distance dependence of the extracted  $G_{BVD}$  is plotted where the distance is given in terms of the wavelength ( $\lambda$ ) calculated at the resonance frequency. While a gradual decline is expected a less than ideal response is observed due to near-field effects, multipath interference and reflections. (b) The distance (given in terms of the wavelength) dependence of the calculated efficiency is plotted. It is observed that the efficiency is initially low. However, it increases with increasing distance, rising to a maximum of 16% at a distance of 1.2 m. (c) The dependence of the Q on distance (in terms of wavelength) is shown. The quality factor varies from between 1400 to about 3600. (d) The superimposed Lorentzian response of the device at distance of 0.15 m and 1.25 m is shown. While the magnitude of the resonance response is higher at 0.15 m, the subsequent quality factor is lower. At 1.25 m, the magnitude is lower and the quality factor is higher, thus resulting in a higher efficiency for the device at 1.25 m than at 0.15 m.

of the efficiency is plotted in Figure 3(b). The efficiency of the device increases to a maximum of nearly 15% at a distance of 1.2 m from the source antenna. The efficiency of the device is given by the ratio of the incident power to the output power, where the incident power is calculated as the product of the measured power density at each distance by a portable handheld power meter (RF-Explorer 3 G) and the effective area of the top IDTs. The output power is calculated from the S21 response of the device measured by the VNA. The efficiency reported here is still low; however, it is significantly larger than the 3% reported by us. The primary reason is believed to be the ratio of device size and wavelength. Increasing this ratio by increasing frequency and at the same time reducing the excitation wavelength can improve the directivity of the device, which can lead to better energy transfer between the incident electric field and the piezoelectric resonator. Typically, the conventional thickness BAW modes have much higher frequencies, which are expected to generate even much higher efficiencies. The quality factors calculated at each distance (given in terms of the wavelength) for the resonator are shown in Figure 3(c) and can be seen to be between 1000 and 4000. Figure 3(d) shows the superimposed Lorentzian response of the device. It demonstrates that while the magnitude of the resonance is higher at 0.15 m (starting distance of the experiment) the quality factor is lower and at 1.25 m (the last distance measured) the quality factor is higher and the magnitude of the resonance is lower. Thus, the device has a lower efficiency at 0.15 m and a higher efficiency at 1.25 m. It may also be noted that a slight shift in the resonance frequency from 356.2 MHz is also observed as the distance is varied between the source antenna and device.

To summarize, we demonstrate wireless actuation of  $S_0$  Lamb wave mode in a micromechanical resonator with 15% efficiency. This enabling technology of low-power excitation

of micromechanical devices with small footprint could be fundamentally important to a wide variety of applications in wireless communication and biomedical device engineering.

Financial support from FemtoDx is acknowledged.

- <sup>1</sup>M. Imboden and P. Mohanty, *Phys. Rep.* **534**, 89–146 (2014).
- <sup>2</sup>A. Gaidarzhy, M. Imboden, P. Mohanty, J. Rankin, and B. W. Sheldon, *Appl. Phys. Lett.* **91**, 203503 (2007).
- <sup>3</sup>P. Mohanty and M. Imboden, in *Nanodiamonds*, edited by O. Williams (Royal Society of Chemistry, London, 2013), Vol. 31, p. 411.
- <sup>4</sup>M. Imboden, O. A. Williams, and P. Mohanty, *Nano Lett.* **13**(9), 4014–4019 (2013).
- <sup>5</sup>J. Dorignac, A. Gaidarzhy, and P. Mohanty, *J. Appl. Phys.* **105**, 103520 (2009).
- <sup>6</sup>C. M. Lin, Y. Y. Chen, V. V. Felmetsger, D. G. Senesky, and A. P. Pisano, *Adv. Mater.* **24**, 2722–2727 (2012).
- <sup>7</sup>J. Biurstrom, I. Katardjiev, and V. Yantchev, *Appl. Phys. Lett.* **86**, 154103 (2005).
- <sup>8</sup>V. Yantchev, J. Enlund, J. Biurstrom, and I. Katardjiev, *Ultrasonics* **45**, 208–212 (2006).
- <sup>9</sup>J. H. Kuypers, C. M. Lin, G. Vigevani, and A. Pisano, in *IEEE International Frequency Control Symposium*, 2008, pp. 240–249.
- <sup>10</sup>H. Zhang, J. Liang, X. Zhou, H. Zhang, D. Zhang, and W. Pang, *IEEE Trans. Electron Devices* **62**(9), 3034 (2015).
- <sup>11</sup>C. M. Lin, V. Yantchev, J. Zou, Y. Y. Chen, and A. P. Pisano, *J. Microelectromech. Syst.* **23**(1), 78 (2014).
- <sup>12</sup>M. Narducci, M. Ferrari, V. Ferrari, and H. Campanella, *Procedia Eng.* **87**, 1152–1155 (2014).
- <sup>13</sup>C. Zuo, J. V. der Spiegel, and G. Piazza, *IEEE Trans. Ultrason., Ferroelectr., Freq. Control* **57**, 82–87 (2010).
- <sup>14</sup>X. Lu, C. M. Lee, S. Y. Wu, H. P. Ho, and K. M. Lau, *IEEE Sens. J.* **13**, 1245–1251 (2013).
- <sup>15</sup>Z. Chen, L. Fan, S. Zhang, and H. Zhang, *Ultrasonics* **65**, 296–303 (2016).
- <sup>16</sup>V. Yantchev and I. Katardjiev, *J. Micromech. Microeng.* **23**, 043001 (2013).
- <sup>17</sup>A. Choujaa, N. Tirole, C. Bonjour, G. Martin, D. Hauden, P. Blind, A. Cachard, and C. Pommier, *Sens. Actuators, A* **46–47**, 179–182 (1995).
- <sup>18</sup>V. Giurgiutiu, *J. Intell. Mater. Syst. Struct.* **16**, 291 (2005).
- <sup>19</sup>F. Mateen, C. Maedler, S. Erramilli, and P. Mohanty, *Nat. Microsyst. Nanoeng.* **2**, 16036 (2016).